ADVANCED MATERIALS INTERFACES
www.advmatinterfaces.de

Structural Modifications in Bilayered Molecular Systems Lead to Predictable Changes in Their Electronic Properties

*Carleen M. Bowers, Minlu Zhang, Yekaterina Lyubarskaya, Eric J. Toone, Ching Tang, and Alexander A. Shestopalov**

This study uses a novel surface engineering approach to demonstrate the influence of organic functional group substitutions on molecular electronic properties. Specifically, bilayered organic monomolecular systems immobilized on an inorganic electrode as the charge-injecting components of organic electronic devices are compared. Recent literature reports demonstrate that structural modification in functional monolayers have unpredictable effects on their electronic properties. These studies indicate that the structure most certainly plays an important role, but its effect on the molecular resistance is diminished due to differences in other monolayer parameters. It is demonstrated that a separate control over the monolayer geometry and its chemical structure is required in order to observe predictable structure-property relations. Here, bilayered molecular interfaces, comprising inert and functional layers whose properties can be independently controlled, are formed. It is shown that 1) the charge transfer through the bilayered system is sensitive to small structural molecular changes; 2) that it can be controlled and predicted by controlling the electron-withdrawing or donating nature of the organic moiety; and 3) that the differences in the charge transfer dynamics of two bilayered systems can be visualized via patterned electroluminescence.

1. Introduction

Molecular electronic (ME) devices, in which single molecules serve as active electronic components, constitute a viable approach for overcoming fundamental downscaling limitations of complementary metal oxide semiconductor technology.[1–4] The long-standing hypothesis is that the structures of molecules positioned inside electrical junctions cause a predictable and controllable effect on the rate and mechanism of charge transport.[5] Previous single-molecule-based ME studies have successfully validated this assumption by demonstrating control over the charge-transport rate, molecular rectification, and molecular orbital gating through structural modifications of molecules positioned inside nanogap and break junction devices.[2,6] However, such studies were specifically designed to probe individual molecules, relying on molecular architectures that cannot be applied in traditional film-based devices. The adaptation of these studies to practical devices based on continuous monolayers is not straightforward, primarily because monolayer-based studies have thus far struggled to demonstrate predictable control over ME properties through functional group substitution. Although multiple reports have demonstrated that the length-variations in non-functional aliphatic[7–10] and perfluorinated[11–14] SAMs lead to predictable changes in molecular resistance, recent studies that compare functional charge-transporting monolayers have demonstrated that structural modifications is such systems have rather unpredictable outcomes, and that changes in the monolayer functionality do not significantly affect charge injection.[15–17] We attribute these findings to variations in other monolayer parameters that affect electronic properties, specifically the density of functional groups, their geometrical orientation, and their vertical position within the junction.[5,18–23] These variations in monolayer properties suggest that it is important to have independent control over the functional group structure from the overall monolayer geometry to effectively regulate ME performance.

Here, we demonstrate independent control over the monolayer functionality from its geometry, and show that structural modifications in these monolayers lead to predictable changes in their ME performance. By using bilayered surface engineering and an organic electronic-based test platform, we demonstrate 1) the construction of well-defined molecular interfaces on indium tin oxide (ITO) electrodes; and show 2) that the charge transfer through these systems is sensitive to small structural changes, and that it can be controlled by controlling the electron-withdrawing or donating nature of the organic moiety. Lastly, we demonstrate 3) that the difference in charge transfer dynamics between two bilayered systems can be visualized via patterned electroluminescence in organic light emitting diodes (OLEDs).

Dr. C. M. Bowers, Prof. E. J. Toone
Department of Chemistry
Duke University
Durham, NC 27708, USA
Dr. M. Zhang, Y. Lyubarskaya, Prof. C. Tang, Prof. A. A. Shestopalov
Department of Chemical Engineering
University of Rochester, Rochester
NY 14627, USA
E-mail: alexander.shestopalov@rochester.edu

DOI: 10.1002/admi.201300109

 © 2014 WILEY-VCH Verlag GmbH & Co. KGaA, Weinheim

ADVANCED MATERIALS INTERFACES
www.advmatinterfaces.de

Materials Views
www.MaterialsViews.com

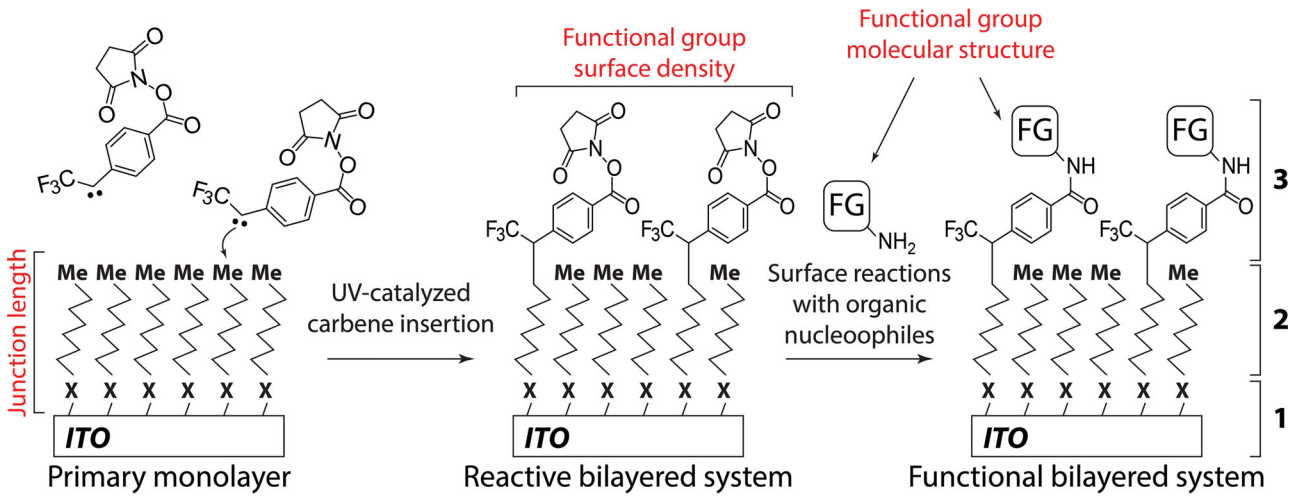

Figure 1. Formation and structure of the bilayered molecular system. 1) The inorganic interface connected to the primary aliphatic monolayer via covalent bonds. 2) The primary monolayer composed of inert long-chain aliphatic molecules. Dense and ordered packing of alkyl chains ensures uniform monolayer thickness and restricts the diffusion of corrosive species to the inorganic-organic interface. The primary monolayer provides support for and ensures uniform geometrical orientation of the secondary layer. 3) The secondary layer is linked to the primary monolayer via stable non-hydrolyzible CH_2–CH bonds. It provides reactivity and function to the bilayered system. Because the primary monolayer is terminated with inert CH_3 groups, the chemical properties of the bilayered system are determined only by the structure of the secondary overlayer. All drawings are not to scale.

2. Bilayered Molecular Interfaces

In this study we used bilayered molecular interfaces that differ only in the structure of the terminal functional group. All other monolayer parameters, such as monolayer density, functional group lateral distribution, and its distance from the inorganic interface, remain the same.[24–27] Our system comprises a dense, inert aliphatic adlayer and a functional organic overlayer that are linked together with non-hydrolyzable CH_2–CH bonds (**Figure 1**). The primary monolayer is composed of highly organized and chemically inert aliphatic molecules. It has properties of inert crystalline organic materials with well-defined packing arrangement, density, and geometrical topology. The secondary overlayer is affixed to the primary monolayer with stable C–C bonds via carbene insertion chemistry. This overlayer comprises closely spaced functionalities that give the interface chemical reactivity or desired physical, electrostatic or HOMO/LUMO properties. In our system, the geometrical position of the functional moiety within the junction and the junction overall length are controlled by the structure of the primary adlayer. The surface density of the functional moieties is determined by the conditions of the UV-catalyzed carbene insertion, while the functional group structure is determined by the molecular structure of the surface reacting molecules.

Our system is different from traditional functional SAMs with disordered aliphatic adlayers. It is also different from bilayered systems that rely on reactive adlayers terminated with small NH_2, COOH, Hal, and N_3 groups. The surface reactions of such SAMs are typically incomplete, leading to the presence of additional electronic states and to unwanted reactivity. Because our primary adlayer is inert, the chemical and electronic properties are determined only by the secondary overlayer.[24] Our approach also avoids the limitations of mixed and backfilled SAMs associated with a low and unpredictable density of functional groups, and with phase separation of inert and functional components (Figure 1SI, Supporting Information).

To demonstrate that geometrical parameters and chemical structure of continuous functional monolayers predictably influence charge transport in electrical junctions, we utilized the bilayered strategy to modify ITO electrodes in OLED devices. We used ordered primary monolayers that have similar organization but different lengths, and secondary overlayers that bear different organic functionalities. Aliphatic organosilanes and phosphonic acids bind strongly to ITO, forming stable crystalline-like monolayers.[28] We used these molecules to create primary C8 and C18 monolayers (**P1**–**P3**) on ITO via standard protocols (**Figure 2**). X-ray photoelectron spectroscopy (XPS) confirmed successful SAM formation (Figure 2b). AFM analysis showed that clean ITO **C1** and primary **P2** and **P3** SAMs have granular morphology and approximately the same roughness values (**P2**(Rz) = 1.45 nm, **P3**(Rz) = 1.60 nm, **C1**(Rz) = 1.66 nm and Figure 2SI). Goniometry measurements confirmed formation of dense hydrophobic monolayers (**P2**(α_{st}) = 106.7°, **P3**(α_{st}) = 97.6°, **C1**(α_{st}) = 58.6°) with relatively high contact angle hysteresis (**P2**(α_{ad}-α_{rec}) = 11.9°, **P3**(α_{ad}-α_{rec}) = 17.1°, **C1**(α_{ad}-α_{rec}) = 15.3°). Both AFM and goniometry data suggest that the created primary SAMs contain relatively large number of boundary defects associated with the granular morphology of ITO. As expected, shorter C8 SAMs demonstrated less uniform organization than C18 monolayers (by goniometry), due to the weaker Van-der-Waals interactions between shorter aliphatic chains.

To form the reactive overlayer, we reacted alkyl modified surfaces **P1**–**P3** with a diazirine-derived carbene, producing a secondary layer bearing *N*-hydroxysuccinimide (NHS) activated esters (**S1**–**S3**, Figure 2). XPS analysis revealed an F1s signal, indicating the successful UV-catalyzed insertion of the

© 2014 WILEY-VCH Verlag GmbH & Co. KGaA, Weinheim

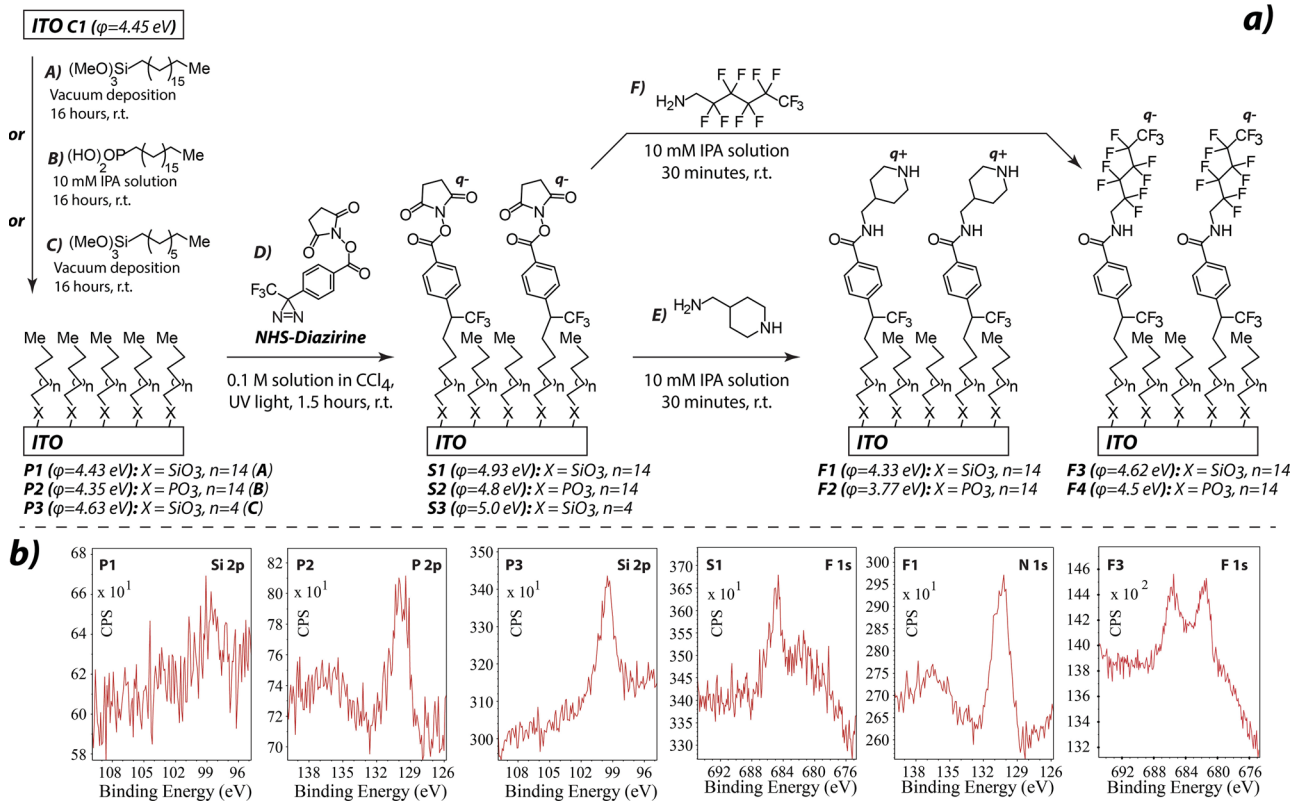

Figure 2. Primary (**P1**–**P3**) and secondary molecular layers (**S1**–**S3**, **F1**–**F4**) on ITO electrodes. a) Surface reactions, molecular structures, conditions, and work function values of **C1**, **P1**–**P3**, **S1**–**S3**, and **F1**–**F4**. b) High-resolution XPS spectra of the primary SAMs **P1**–**P3** (demonstrate the presence of Si2p and P2p electrons in monolayers of aliphatic organosilanes and phosphonic acids); of the secondary overlayer **S1** (demonstrate the presence of F1s electrons following UV catalyzed carbene insertion of CF_3-containing NHS-diazirine); and of piperidine (**F1**) and perfluoroalkyl (**F3**) functionalized sec ondary overlayers (demonstrate the presence of N1s (**F1**) and additional F1s (**F3**) electrons). XPS spectra of the clean ITO substrate (**C1**) lack Si2p, P2p, F1s, and N1s signals. All drawings are not to scale.

NHS-diazirine to the methyl terminated surfaces (Figure 2b). This molecular architecture provides a general template that can be further modified to provide functionality via standard surface reactions. To demonstrate molecular control over the charge-transfer dynamics, we functionalized reactive bilayered substrates **S1**,**S2** with two organic species—electron-donating piperidine molecules (**F1**,**F2**) and electron-withdrawing perfluorinated alkyls (**F3**,**F4**)—which exhibit opposing dipole moments when positioned away from the interface (Figure 2).

Following formation of bilayered systems on ITO, we analyzed how their molecular and geometrical properties affect electrode's work function. Literature reports suggest that polar or electrostatic SAMs can change the work function of the electrode by shifting up or down the vacuum level with the surface oriented dipole moment.[29–32] Thus, polar moieties can be used to increase or decrease the work function through their electron-withdrawing or donating properties and by controlling their distance from the electrode. However, beside affecting the dipole moment value, the SAM total thickness also affects the charge tunneling distance and may lead to lower current densities in electrical junctions with long aliphatic components.[33] Ultraviolet photoelectron spectroscopy (UPS) measurements of bilayered substrates **S1**–**S3**, **F1**–**F4** demonstrated that combining a short alkyl spacer with a strong electron-withdrawing group leads to the highest work function value (**S3**ϕ = 5.0 eV); increasing the distance between the functional group and the electrode surface slightly decreases the work function (**S1**ϕ = 4.93 eV, **S2**ϕ = 4.8 eV); increasing the total length of the bilayered system further decreases the work function (**F3**ϕ = 4.62 eV, **F4**ϕ = 4.5 eV); and the incorporation of electron-donating moieties significantly lowers the work function by inverting the orientation of the surface dipole moment (**F1**ϕ = 4.33 eV, **F2**ϕ = 3.77 eV). These findings suggest that control over the monolayer length and structure is needed to regulate the work function, and that such geometrical and structural control can be achieved with the bilayered approach.

3. Organic Electronic Test Platforms

In this work we used a standard OLED device to compare the hole-injection properties of bilayered systems (Figure 3SI, Supporting Information). By utilizing this traditional OE architecture, we demonstrate that SAM-based OE devices constitute a practical and reliable alternative to traditional ME test platforms, and that the electronic properties of the monolayer components can be distinguished and compared through the analysis of typical OLED parameters (e.g., drive voltage and

 © 2014 WILEY-VCH Verlag GmbH & Co. KGaA, Weinheim

luminance). This is possible due to several distinctive features of OE devices: 1) they include an organic conducting thin film positioned on top of the monomolecular layer. This film protects the monolayer from other device components, and reduces the impact of SAM-related defects on the charge-tunneling by filling the defect sites with organic molecules of comparable resistivity. 2) The constant macroscopic (≈3 mm × 3 mm) device area ensures the same uniform distribution in the number of the SAM-related defects on all tested devices, averaging their impact on the device performance. 3) The devices are fabricated and analyzed using well-established automated protocols, making the data collection independent from the operator.

OLED fabrication was carried out in a custom-built vacuum chamber operating at a base pressure of ≈ 3×10^{-7} Torr. The detailed OLED layer structure is as follows: ITO/anode buffer layer (**P**,**S**,**F**, or **C**)/*N*,*N*′-dinaphthalene-1-yl-*N*,*N*′-diphenyl-benzidine (NPB)/tris(8-hydroxyquinolinato)aluminum (Alq_3)/bathophenanthroline (Bphen)/LiF/Al. The device active area was 0.1 cm^2, defined by the overlapping area of the ITO and Al electrodes. All OLED parameters (drive voltage, luminance and efficiency) were measured and averaged on at least four different devices and no data points were excluded from the analysis. All fabricated devices were functional. Shown in **Figure 3** are device performance parameters (drive voltage and luminance measured at a constant current of 20 mA cm^{-2}) for a set of OLEDs with various organic monolayers. The principle metrics used in this study are the work function ϕ of the monolayer-modified ITO electrode and the drive voltage V_d of the OLED device evaluated at different current densities. The hole injection barrier at the ITO interface depends on the local work function of the ITO anode. This barrier and the device drive voltage can be significantly reduced by increasing the ITO work function and by bringing it closer to the HOMO level of the NPB hole-transport layer. Thus, low V_d and high ϕ values indicate an increased hole-transfer rate from the ITO electrode to the organic charge-transporting thin film, assuming that all other device parameters stay the same.

Figure 3 shows that the performance of the fabricated OLEDs is sensitive to the terminal organic functionality of the bilayered system. Drive voltage data confirms that electron donating piperidine moieties in **F1** and **F2** repel holes and hinder their injection from the ITO electrode. On the other hand, electron-withdrawing NHS esters in **S1**–**S3** and perfluorinated alkyl moieties in **F3** and **F4** attract negative charges to the ITO anode and facilitate anodic hole-injection into the NPB layer. Also plotted in Figure 3 are the effective work functions of the anodes. As expected, the OLED drive voltage and the work function of the modified ITO anode exhibit an inverse relationship with each other. Moreover, almost all OLEDs modified with the electron-withdrawing functional groups (**S1**,**S3**,**F3**,**F4**) demonstrated lower drive voltage values than the device modified with a MoOx layer (V_d = 7.68 V), which is currently considered one of the most efficient hole-injecting materials.[34] In contrast, the luminance bears little correlation with the work function of the anodes. The nominal luminance is about 1000 +/– 200 cd m^{-2} except for **P1**, which has a luminance below 400 cd m^{-2}. The lower luminance output for **P1** may be attributed to the increased quenching at the ITO

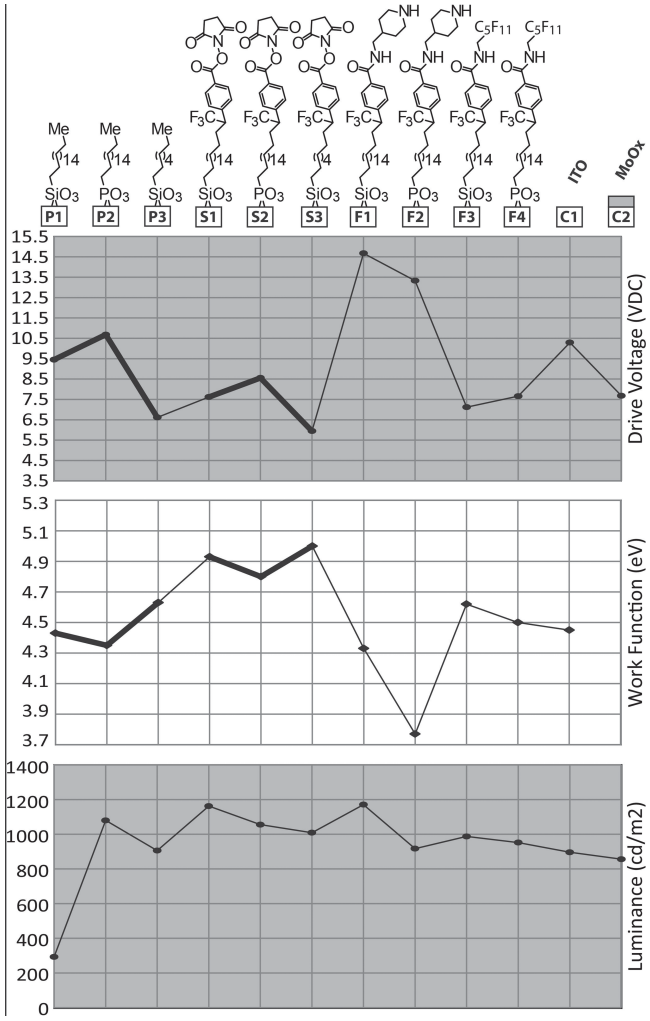

Figure 3. Molecular components and working parameters of the bilayered OLED devices: drive voltage, work functions, and luminance. Bold lines indicate similar trends between **P1**-**P3** and **S1**-**S3** devices. All drawings are not to scale.

anode surface for reasons which are unclear at this moment. Similar luminance values among tested devices, including the untreated ITO **C1** and MoOx-modified **C2**, indicate that the quenching effect at the ITO surface is avoided and that the electron-hole recombinations presumably occur further from the ITO surface. This observation suggests that the molecular systems on ITO have no effect on other device parameters (e.g., position of the recombination zone), and that they only influence the rate of charge transfer from the ITO electrode to the hole-transporting NPB film. This confirms that SAM-based OE devices, despite their more complex architectures, can be used to probe the same charge transfer properties as traditional ME test platforms.

Analysis of the drive voltage trends of **P1**–**P3**, **S1**–**S3**, and **F1**–**F4** devices indicate the dependence of the charge-transfer rate from the functional group substitution and from the overall monolayer thickness. For example, **P3** modified with the shorter C8 SAM has a lower drive voltage than **P1** and **P2**

© 2014 WILEY-VCH Verlag GmbH & Co. KGaA, Weinheim

modified with the longer C18 SAMs (in agreement with the elastic tunneling model). The same trend is also visible in **S1**–**S3** devices, where among all bilayered substrates bearing the NHS group, **S3** device with the shortest molecular system demonstrates the lowest drive voltage and the highest rate of charge injection (Figure 3, bold lines). The difference in drive voltages between **P1**–**P2** (and also **S1**–**S2**) can be attributed to a higher molecular density of the phosphonic acid-based SAMs compared to the silane-based SAMs. Higher density SAMs have smaller tilt angles and greater thicknesses, increasing the overall length of the tunneling barrier.

The comparison of simple aliphatic **P1**–**P3** devices and bilayered **S1**–**S3** devices shows that the presence of the organic functional group affects both the rate and mechanism of charge-transfer. Despite the overall increase in the charge-tunneling distance, **S1**–**S3** devices, which bear an electron-withdrawing NHS group, have lower drive voltages than purely aliphatic **P1**–**P3 devices**, suggesting a potential molecular orbital coupling of the tunneling charges within the bilayered system. However, because **P1**–**P3** and **S1**–**S3** series demonstrate the same trend in the V_d dependence on the overall length of the molecular system (e.g., the shortest **P3**,**S3** have the lowest V_d, and the longest **P2**,**S2** have the highest V_d), the elastic charge tunneling should still play an important role in the charge transfer through the functional bilayered system. These findings indicate that the small differences in geometrical properties of SAMs positioned inside the electrical junctions can have an impact on the charge-transfer rate by changing the length of the tunneling barrier, and that the presence of functional groups with narrow HOMO/LUMO gaps can have an effect on the overall mechanism of charge transfer. The comparison of **S1**,**S2** with **F1**,**F2** and **F3**,**F4** indicates that the molecular structure of the terminal functional group in the monolayers, which otherwise have the same surface densities, geometrical properties, and surface-attachment groups, has an obvious effect on the rate of charge injection from the ITO anode to the hole-conducting NPB film. It also shows that the electron-withdrawing or donating nature of the terminal functionality can be used to control and even enhance the hole-injection in bilayered OLEDs. The drive voltage trends of **P1**–**P3**,**F1**–**F4** are also present in their work function values (with the exception of **F1**), providing additional evidence that the molecular structure and geometry of the organic monolayer have clear correlation with its charge-transporting properties.

4. Patterned Electroluminescence

One of our objectives was to demonstrate that OE devices can provide an additional metric with which to compare molecular electronics properties. Here, we show that OLEDs, containing ITO anodes with patterned bilayered systems, exhibit patterned electroluminescence due to the different rates of hole-injection into the emissive layer through the patterned molecules. This experiment serves as additional evidence that the terminal organic functionality in the monomolecular system has a clear effect on the rate of charge transport, since all other parameters of the patterned devices, including the structure of the primary monolayer, stay the same.

To create patterned bilayers on ITO we used catalytic and reactive microcontact printing methods. These techniques are fast, accurate, and inexpensive approaches to pattern preformed, functional monolayers on diverse inorganic substrates, including the bilayered systems on ITO.[24–27,35,36] Catalytic microcontact printing was used to pattern ITO with molecules containing NHS-activated and free carboxylic acid groups. Such patterns were formed by bringing freshly prepared NHS-terminated ITO surface **S1** into conformal contact with a catalytic elastic stamp bearing ~8 μm features. The stamp, bearing covalently bound sulfonic acids, initiated catalytic pattern-specific hydrolysis of NHS-groups, converting them into free carboxylic acids (**G1**, **Figure 4**a). Reactive microcontact printing was used to site-specifically immobilize molecules containing electron-withdrawing and donating groups on ITO. Molecules were selected to maximize both hole injection blocking (4-(aminomethyl)piperidine: **F1**,**F2**) and enhancement (1H,1H-perflurohexylamine: **F3**,**F4**) into the hole-transporting layer. Piperidine- and NHS-terminated SAMs on ITO were first formed by bringing freshly prepared NHS-terminated ITO surface **S2** into conformal contact with a 4-(aminomethyl)piperidine-inked stamp for 1 minute at room temperature. Upon removal of the reactive stamp, surface **G2** was reacted with a 10 mM solution of 1H,1H-perfluorohexylamine in isopropanol for 30 minutes, producing **G3** with chemically distinct patterns of electron-donating and electron-withdrawing groups (Figure 4a).

Prepared patterned substrates were converted into Alq3-based OLEDs (Figure 4b). In these devices, spatially segregated moieties with differing electronic structures create anode areas with different hole-injection properties. These areas determine the rate of charge injection into the hole-transmitting (NPB) and light-emitting (Alq3) layers, creating patterns of bright and dim electroluminescence in the otherwise uniform Alq3 layer. Pattern contrast depends on the hole injection rate and should increase as the differences in the molecular resistivity increases. This prediction was borne out by experiment (Figure 4b). Substrate **G3**, which contained a pattern of electron-donating and electron-withdrawing molecules, showed much higher electroluminescent contrast than did sample **G1**, which bore a pattern of molecules with more similar structures. Our results demonstrate that contrast in patterned OLEDs is predictably adjusted through modification of chemical structures, and that even small structural change (e.g., between NHS and COOH groups) can be distinguished using this test platform. The OLED light intensity is directly proportional to its current density. Conceptually, patterned OLEDs represent parallel resistors that differ only in the chemical structure of the molecular components, making simple molecular resistivity calculations possible. In our future studies, we will use this concept to create molecular OLED arrays that permit fast combinatorial screening of molecular electronics properties by comparing emitted light intensities of the array components.

5. Conclusions

We demonstrated that a bilayered functionalization strategy is a promising approach towards the construction of structured and robust inorganic–organic interfaces with tunable charge

 © 2014 WILEY-VCH Verlag GmbH & Co. KGaA, Weinheim

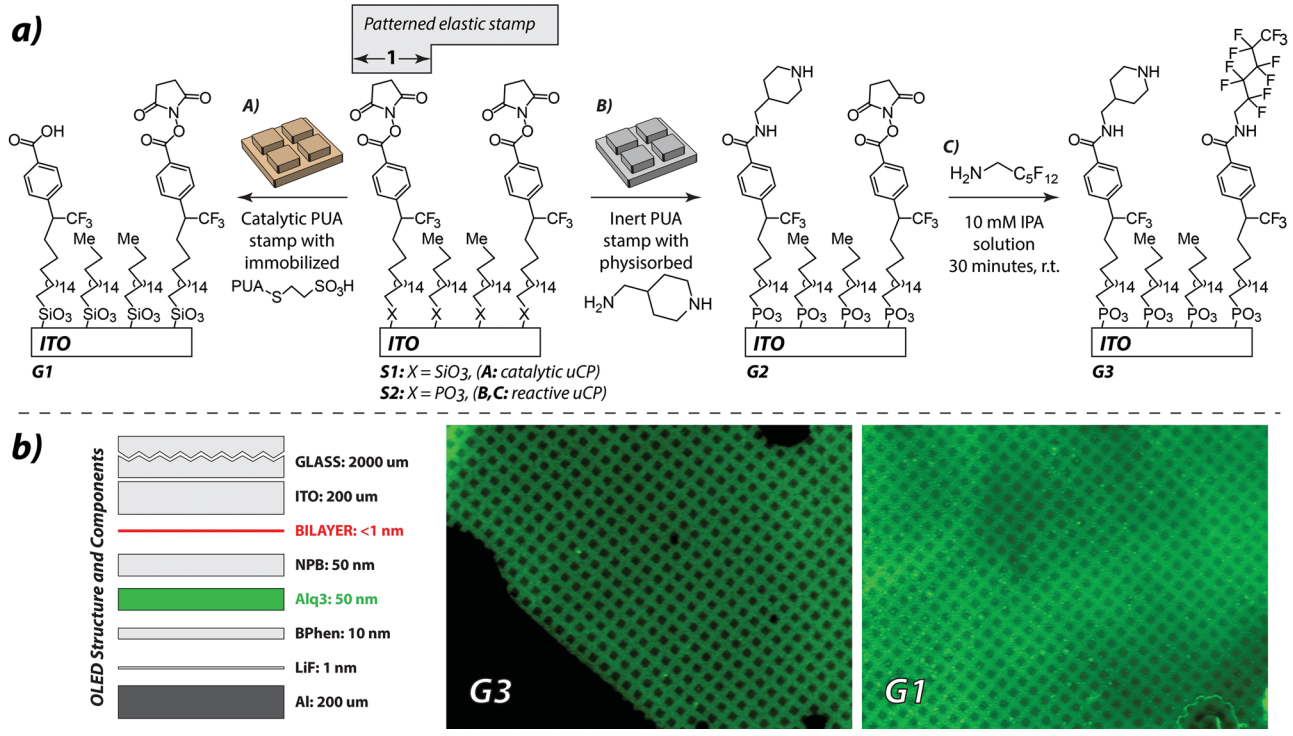

Figure 4. a) Chemoselective soft-lithographic patterning and b) electroluminescence of bilayered OLEDs. a) Catalytic (**A**) and reactive (**B**) microcontact patterning of hole-injecting layers: molecular structures and surface reaction conditions. b) OLED structure and components; optical micrographs of working OLED devices **G3** and **G1** containing patterned hole-injecting layers. All drawings are not to scale.

transporting properties. We have also shown that traditional organic electronics architectures can be used as sensitive and practical platforms for investigating molecular electronics properties. This study shows the dependence of the rate of charge tunneling from the functional group substitution, and provides a simple test platform for comparing electronic properties of functional organic monolayers.

Supporting Information

Supporting Information is available from the Wiley Online Library or from the author.

Acknowledgment

This work was supported by UofR ChemE Startup and in part by the NSF awards DMR-1228889 and CMMI-1000724.

Received: November 11, 2013
Revised: December 18, 2013
Published online: February 6, 2014

[1] J. R. Heath, *Annu. Rev. Mater. Res.* **2009**, *39*, 1–23.
[2] H. Song, M. A. Reed, T. Lee, *Adv. Mater.* **2011**, *23* (14), 1583–1608.
[3] A. Coskun, J. M. Spruell, G. Barin, W. R. Dichtel, A. H. Flood, Y. Y. Botros, J. F. Stoddart, *Chem. Soc. Rev.* **2012**, *41* (14), 4827–4859.
[4] M. Halik, A. Hirsch, *Adv. Mater.* **2011**, *23* (22–23), 2689–2695.
[5] A. Aviram, M. A. Ratner, *Chem. Phys. Lett.* **1974**, *29* (2), 277–83.
[6] H. Song, Y. Kim, Y. H. Jang, H. Jeong, M. A. Reed, T. Lee, *Nature* **2009**, *462* (7276), 1039–1043.
[7] H. B. Akkerman, P. W. M. Blom, L. D. M. de, B. B. de, *Nature* **2006**, *441* (7089), 69–72.
[8] M. M. Thuo, W. F. Reus, C. A. Nijhuis, J. R. Barber, C. Kim, M. D. Schulz, G. M. Whitesides, *J. Am. Chem. Soc.* **2011**, *133* (9), 2962–2975.
[9] W. F. Reus, C. A. Nijhuis, J. R. Barber, M. M. Thuo, S. Tricard, G. M. Whitesides, *J. Phys. Chem. C* **2012**, *116* (11), 6714–6733.
[10] A. Jedaa, M. Burkhardt, U. Zschieschang, H. Klauk, D. Habich, G. Schmid, M. Halik, *Org. Electron.* **2009**, *10* (8), 1442–1447.
[11] U. Kraft, U. Zschieschang, F. Ante, D. Kalblein, C. Kamella, K. Amsharov, M. Jansen, K. Kern, E. Weber, H. Klauk, *J. Mater. Chem.* **2010**, *20* (31), 6416–6418.
[12] U. Zschieschang, F. Ante, M. Schlörholz, M. Schmidt, K. Kern, H. Klauk, *Adv. Mater.* **2010**, *22* (40), 4489–4493.
[13] M. Wang, I. G. Hill, *Org. Electron.* **2012**, *13* (3), 498–505.
[14] S. P. Pujari, A. E. van, O. Yaffe, D. Cahen, T. Weidner, R. C. J. M. van, H. Zuilhof, *Langmuir* **2013**, *29* (2), 570–580.
[15] H. J. Yoon, N. D. Shapiro, K. M. Park, M. M. Thuo, S. Soh, G. M. Whitesides, *Angew. Chem., Int. Ed.* **2012**, *51* (19), 4658–4661, S4658/1-S4658/23.
[16] M. M. Thuo, W. F. Reus, F. C. Simeone, C. Kim, M. D. Schulz, H. J. Yoon, G. M. Whitesides, *J. Am. Chem. Soc.* **2012**, *134* (26), 10876–10884.
[17] S. Y. Sayed, A. Bayat, M. Kondratenko, Y. Leroux, P. Hapiot, R. L. McCreery, *J. Am. Chem. Soc.* **2013**, *135* (35), 12972–12975.
[18] C. A. Nijhuis, W. F. Reus, G. M. Whitesides, *J. Am. Chem. Soc.* **2010**, *132* (51), 18386–18401.
[19] R. M. Metzger, *Chem. Rev.* **2003**, *103* (9), 3803–3834.
[20] W. J. Shumate, D. L. Mattern, A. Jaiswal, D. A. Dixon, T. R. White, J. Burgess, A. Honciuc, R. M. Metzger, *J. Phys. Chem. B* **2006**, *110* (23), 11146–11159.

© 2014 WILEY-VCH Verlag GmbH & Co. KGaA, Weinheim

[21] H. Yu, Y. Luo, K. Beverly, J. F. Stoddart, H.-R. Tseng, J. R. Health, *Angew. Chem., Int. Ed.* **2003**, *42* (46), 5706–5711.
[22] P. E. Kornilovitch, A. M. Bratkovsky, R. Stanley Williams, *Phys. Rev. B* **2002**, *66* (16), 165436.
[23] G. J. Ashwell, W. D. Tyrrell, A. J. Whittam, *J. Am. Chem. Soc.* **2004**, *126* (22), 7102–7110.
[24] A. A. Shestopalov, C. J. Morris, B. N. Vogen, A. Hoertz, R. L. Clark, E. J. Toone, *Langmuir* **2011**, *27* (10), 6478–6485.
[25] C. M. Bowers, E. J. Toone, R. L. Clark, A. A. Shestopalov, *J. Vis. Exp.* **2011**, *58*, 1–7.
[26] C. M. Bowers, A. A. Shestopalov, R. L. Clark, E. J. Toone, *ACS Appl. Mater. Interfaces* **2012**, *4* (8), 3932–3937.
[27] C. J. Morris, A. A. Shestopalov, B. H. Gold, R. L. Clark, E. J. Toone, *Langmuir* **2011**, *27* (10), 6486–6489.
[28] B. M. Silverman, K. A. Wieghaus, J. Schwartz, *Langmuir* **2005**, *21* (1), 225–228.
[29] S. Khodabakhsh, D. Poplavskyy, S. Heutz, J. Nelson, D. D. C. Bradley, F. Murata, T. S. Jones, *Adv. Funct. Mater.* **2004**, *14* (12), 1205–1210.
[30] F. Nuesch, L. SiAhmed, B. Francois, L. Zuppiroli, *Adv. Mater.* **1997**, *9* (3), 222.
[31] C. Ganzorig, K. J. Kwak, K. Yagi, M. Fujihira, *Appl. Phys. Lett.* **2001**, *79* (2), 272–274.
[32] T. Watanabe, M. Fujihira, *Ultramicroscopy* **2009**, *109* (8), 1035–1039.
[33] B. Choi, J. Rhee, H. H. Lee, *Appl. Phys. Lett.* **2001**, *79* (13), 2109–2111.
[34] J. Meyer, S. Hamwi, M. Kröger, W. Kowalsky, T. Riedl, A. Kahn, *Adv. Mater.* **2012**, *24* (40), 5408–5427.
[35] A. A. Shestopalov, R. L. Clark, E. J. Toone, *J. Am. Chem. Soc.* **2007**, *129*, 13818–13819.
[36] A. A. Shestopalov, R. L. Clark, E. J. Toone, *Nano Lett.* **2010**, *10*, 43–46.

 © 2014 WILEY-VCH Verlag GmbH & Co. KGaA, Weinheim